Hindawi
International Journal of Aerospace Engineering
Volume 2020, Article ID 1976208, 10 pages
https://doi.org/10.1155/2020/1976208

Research Article

Improving the Slippage Resistance of Successors of the Mars Instrument "Heat Flow Property Package Instrument" (HP^3) Using Bekker's Spaced-Linked Track

Siebo Reershemius

German Aerospace Center (DLR), Institute for Space Systems, 28359 Bremen, Germany

Correspondence should be addressed to Siebo Reershemius; siebo.reershemius@dlr.de

Received 20 February 2020; Revised 18 May 2020; Accepted 2 June 2020; Published 20 July 2020

Academic Editor: Hikmat Asadov

The "Heat Flow Property Package Instrument" (HP^3) is part of NASA's current Mars mission "InSight", which was launched in 2018 and currently operates on the surface of Mars. The instrument needs to remain at its initial position and orientation during operation. Although the landing site can have significant tilt and can be covered with low cohesion soil, any mechanical excitation might make the instrument slip. Therefore, the instrument is using a tailored feet design, which can withstand lateral loads. Future instruments might require higher resistance against slip. This can be due to stronger tilted landing sites or due to higher shocks emitted from stronger penetration probes. This paper introduces a novel design for those instruments based on the idea of the "spaced-link track" of Bekker to further minimize slippage. This design concept is originally used on tracks of heavy machinery. It is presented how the major design feature can be incorporated into the current design. A newly developed analytical-numerical model is utilized to estimate the track force of the new design. The paper closes with a design study at which the new design and the current design are compared to each other for different sized feet.

1. Introduction

The "Heat Flow Property Package Instrument" (HP^3) [1] is used to measure the temperature gradient of the Martian crust using a hammering penetration probe. The instrument is part of NASA's current Mars mission "InSight" [2], which was launched in 2018 (see also Figure 1). The instrument is deployed by a robotic arm [3] to the surface of Mars. Afterwards, it operates mechanically independent from the lander on the surface. A tailored feet design [4] ensures position stability on the surface during the hammering of the penetration probe. The current feet design provides sufficient track resistance for this mission. The slippage resistance needs to be increased for future missions due to potentially stronger penetration probes or stronger tilted landing sites. Complexity level and mass shall remain similar to be in accordance to the mission requirements. The HP^3 instrument uses four, rigid, circular feet as contact interface to the soil. The design resembles a turned-around cup. The paper studies the modification of the current shape by incorporating design elements of the "spaced-link track". The spaced-link track concept was introduced by Bekker [5] in the 1960s. He showed that heavy agricultural and military machinery equipped with spaced-link tracks can have significantly better performance as others with conventional tracks on soft ground. Though it is studied within this paper, how the performance of the feet increases, if the design is adapted to a spaced-link track design. The paper starts with the introduction of Bekker's spaced-link track and its analytical track force estimations. Though the analytical equations are more convenient to be used, they use empirical factors derived for large scale applications under earth gravity. Hence, a new numerical model based on the FEM is introduced, which can be scaled to different gravities and dimensions. The paper continues with the presentation of the new design incorporating Bekker spaced-link track. (Semi-)analytical models to estimate the slippage resistance are derived for both designs. Those are used to study the theoretical performance of the designs. The paper closes with the presentation of the results and the final recommendation for further proceeding.

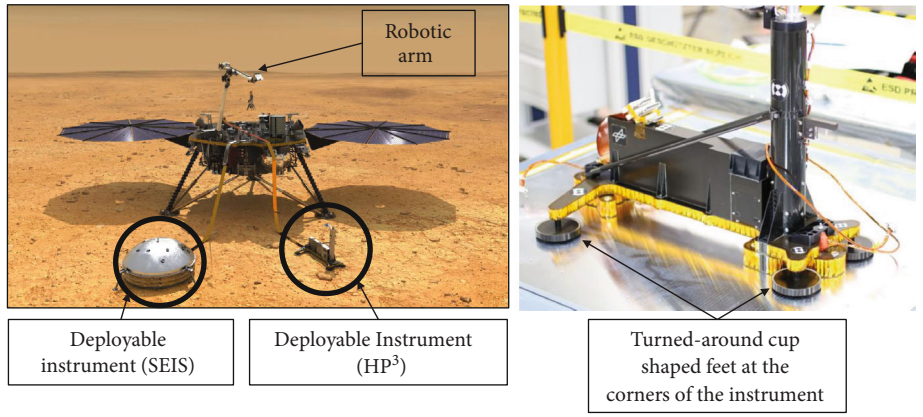

Figure 1: Left: artist's illustration of the InSight lander on the surface of Mars (Image Credit: NASA/JPL [6]). Right: the HP^3 instrument flight-model in DLR cleanroom environment.

2. Bekker's Spaced-Link Track

Tracks are used on heavy machinery to ensure their mobility on soft or muddy terrain. They provide enough resistance against sinkage due to their large contact area. Their blades penetrating the soil ensure forward traction. Research on the shape of those tracks is done since the beginning of the last century. In the 60s, Bekker published his idea of a differently designed track called the "spaced-link track" [5]. Bekker showed that vehicles equipped with those tracks can generate significantly more traction. At that time, tracks used on earth-moving machinery or tanks are based on L-shaped cleats, which are arranged very close to each other (Figure 2(a)). Bekker discovered that a track can have a significant higher track force if the distance between the cleats is increased until the resulting shear failure area is not interfering with any other cleat. Figure 2 shows the comparison between a conventional track and a spaced-link track. It can be seen that the total rupture area of the spaced-link track in front of the cleat is larger than on a conventional one. A larger soil rupture area increases the track force significantly. This effect is mainly driven and influenced by the combination of the gravitational pressure and the horizontal pressure on the cleat during track.

2.1. Analytical Analysis of Bekker's Spaced-Link Track. Bekker derived analytical equations for a spaced-link track based on the logarithmic spiral method in combination with a virtual wall. He assumed that the horizontal track force (H) and the vertical weight-force (W) lead to a virtual wall, from which he could derive the reaction forces based on Terzaghi [7] passive earth pressure theory. He used a logarithmic spiral curve starting from the bottom of this wall to derive the total length l_s. The analytical equations are based on individual soil properties and the geometry of the foot and cleat. The soil properties are the specific weight (γ), cohesion (c), and friction angle (ϕ). The geometry of the foot is represented by the total length (l_{total}) and the total width (b_s). As it can be seen in Figure 3, the cleats are specified by the height (h_s) and the length (s_s). Hereafter, Bekker's equations presented in [5] are repeated without derivation. A detailed derivation of the equations can be found in [5]. The total track force (H_{total}) of one track is given by:

$$H_{\text{total}} = N_s b_s s_s \left(c n_c + \gamma z_j n_q + \gamma n_q \left(\frac{W}{N_s b_s s_s k_s} \right)^{1/n} + \frac{1}{2} \gamma s_s n_\gamma \right) \sin(\theta) + 2\Delta H, \tag{1}$$

to complete the calculation one needs to include the additional track force (ΔH) from shear stresses at both ends of the track:

$$\begin{aligned} \Delta H = N_s \gamma \Bigg(\Bigg(\Bigg(\pi l_s^3 (90 - \phi) \tan 45 - \frac{\phi}{2} \Bigg) \Bigg) \Bigg) /540 + \pi z l_s^2 (90 - \phi)/180) \\ \cdot \tan \left(\left(45 + \frac{\phi}{2} \right) \right) + c l_s^2 (90 - \phi)/180 + c l_s^2 \tan((45 + \phi/2)) \\ \cdot \cos \left(\left(45 - \frac{\varphi}{2} \right) \right). \end{aligned} \tag{2}$$

Furthermore, the total sinkage of the track z, which is a combination of the initial sinkage z_s and the sinkage during track z_j, must be also considered.

$$\begin{aligned} z &= z_j + z_s \\ z_j &= \frac{j \left(W - N_s b_s s_s \left(c N_c + N_q \gamma (W / N_s b_s k_s)^{1/n} + 1/2 \gamma s_s N_\gamma \right) \right)}{H_{total} + N_s N_q b_s s_s j}. \\ z_s &= \left(\frac{W}{N_s b_s s_s \left((k_c / s_s) + k_\phi \right)} \right)^{1/n} \end{aligned} \tag{3}$$

The number of cleats on a track (N_s) is given by:

$$N_s = \frac{l_s + l_{\text{total}}}{l_s + s_s}. \tag{4}$$

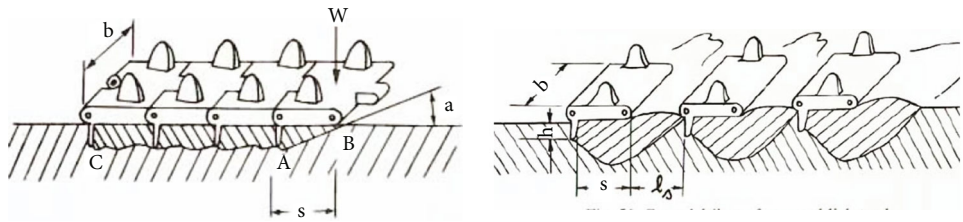

Figure 2: Comparison between a conventional track (a) and Bekker's spaced-link track (b). Figures taken from [5].

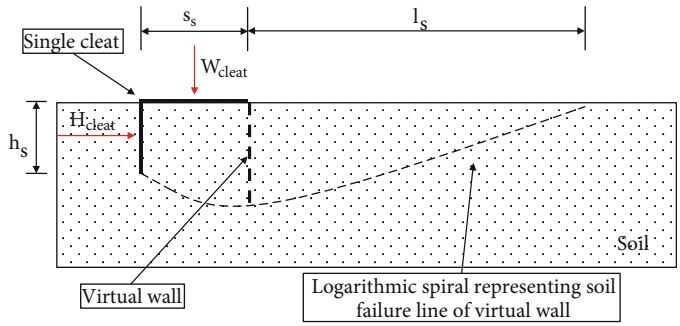

Figure 3: Description of the geometrical parameters, virtual wall, and the rupture line of a single cleat.

θ represents the resulting force angle, which is defined by:

$$\theta = \arctan\left(\frac{H_{\text{total}}}{W}\right). \tag{5}$$

The total length of the rupture area (l_s) can be derived using:

$$l_s = \frac{s_s \exp\left(270 - 2\theta - \phi\right)/114.6 \tan\left(\phi\right)\left(\cos\left(\theta\right) + \left(h_s/s_s\right)\sin\left(\theta\right)\right)}{\sqrt{2}\left(\cos\left(\phi/2\right) - \sin\left(\phi/2\right)\right)}. \tag{6}$$

N_s, N_γ, and N_q are experimentally determined and published by Bekker in [5]. Additionally, the coefficients n_c, n_q, and n_γ are used, which are experimental parameters from Terzaghi passive earth pressure method published in [7]. The total track resistance H_{total} cannot be directly derived from equation (1) as H_{total} is also needed to derive z_j. Therefore, Bekker proposed an iterative solution process, at which the total slippage and the spacing l_s is assumed prior to calculation. The iterative solution will be recapped here for completeness:

(i) Assume slippage j and l_s

(ii) Calculate z_s using equation (3)

(iii) Assume one value for H_{total}

(iv) Calculate z_j using using equation (3), θ using equation (5), z using equation (3) and ΔH using equation (2)

(v) Calculate new H_{total} using equation (1)

(vi) Compare the assumed and calculated values for H_{total}. Change the assumption and repeat step 2. to 5. until $(H_{\text{assumed}} - H_{\text{calculated}}/H_{\text{calculated}}) < \epsilon$. At which ϵ is chosen between 0.01 and 0.05

2.2. Finite Element Analysis of Bekker's Spaced-Link Track. Bekker's analytical expressions for the force generated by a track and the spacing between the cleats were shown in the previous chapter. Though the analytical equations are more convenient to be used, they use empirical factors derived for large scale applications under earth gravity. Hence, a new numerical model based on the FEM is introduced, which can be scaled to different gravities and dimensions. Since the time Bekker derived these equations, numerical methods were developed extensively. Therefore, it became a usual practice to use those to investigate even more complex problems. One of those methods is the Finite Element Method in combination with an elasto-plastic material model. Many researchers [8–10] did apply this numerical method to their problems and validated its general applicability. Therefore, this publication continues using a finite element model of the spaced-link track to determine the needed design parameters for the foot. The FEM model represents a two-dimensional model of one cleat in order to reduce complexity. The total track force is derived analytically by extrapolation.

2.2.1. Material Model of the Finite Element Model. Material elasticity is based on the isotropic material parameter of the soil. Plasticity is incorporated by including a failure criterion to define a limit for the elasticity behavior, a flow rule, which gives the stress-strain relationship in a plastic state and a consistency criterion to avoid that stress is exceeding the yield

limit. Failure criteria can be generalized as a closed surface in three-dimensional principal stress space (see [11]). There are various failure criterions available in the literature, which are usually based on the parameters of the Mohr-Coulomb model. For example, see [12–16]. One of them is the Drucker-Prager failure criterion proposed by Drucker and Prager in 1952 [17]. It is similar to the von-Mises failure criteria, but does additionally account for the influence of the hydrostatic pressure [11]. This criterion is widely implemented in numerous commercial finite element software packages as it has a conical shape in the three-dimensional stress space, which can be integrated into numerical solvers easily. The Drucker-Prager material model is defined in the three-dimensional stress-space as follows:

$$\sqrt{\frac{1}{6}\cdot\left[(\sigma_1-\sigma_2)^2+(\sigma_2-\sigma_3)^2+(\sigma_3-\sigma_1)^2\right]} = A + B\cdot(\sigma_1+\sigma_2+\sigma_3) \tag{7}$$

The parameters A and B are defined in relation to the Mohr-Coulomb failure criterion. In literature, they are defined such that the cone of the Drucker Prager failure criterion inscribes, middle-circumscribes, or circumscribes the hexagonal-shaped cone of the Mohr-Coulomb failure criterion [16]. The mathematical formulation of the parameters can be found in Table 1 derived from [18].

For the numerical analysis, the inscribing configuration of the Drucker-Prager parameter conversion is chosen, as it provides the best fit to the measurements.

2.2.2. Modelling of Bekker's Spaced-Link Track. The numerical modelling is performed in ANSYS 16.0. The analysis approach is used by [8, 9], or [10] and is common practice for such soil problems.

(1) Model Description. A fully parametrized 2D FEM model is developed for ANSYS Mechanical to determine the total reaction force of one cleat. The model assumes that the height of the cleat in the soil is much smaller than the total width of the track. The mesh has a shape of a rectangular surface with a cut-out at the upper left corner. The total mesh dimensions depend on the height of the cleat: the total width is ten times the lengths (s_s) of the cleat; the total height is five times the depth (h_s) of the cleat. The element size at the outer edges of the mesh is chosen very coarse (about 1/10 height of cleat). The element size is reduced drastically towards the upper side (+Y) of the model to increase accuracy at the area, where the highest stresses are expected. At the corners of the cut-out, which is also in contact with the cleat, the element size is additionally reduced to reduce singularity effects. Figure 4 shows an overview of the FEM model with its refined mesh and the boundary conditions. The displacements of the nodes at the +X, -X, and -Y sides of the model are blocked towards the orthogonal direction of the edge. The nodes at the -Y side of the cut-out are assigned to have a constant displacement towards -Y direction in order to ensure a homogenous stress field without the need of an additional rigid body, which might interfere with the blade body at the corner of the cut-out. The soil is modeled as an elastic-plastic Drucker-Prager material with associated flow rule. The properties of the soil can be found in Table 2. The displacement of the cleat and gravity are applied to the mesh simultaneously. The soil is represented by triangular PLANE183 elements. Rigid bodies are modeled using a MASS21 point mass and CONTA172/TARGE169 elements. Figure 5 illustrates the modelling of a single cleat in soil. The cleat is modeled by two rigid bodies. One rigid body represents the vertical part of the cleat (rigid body number 1 in the figure), and the second rigid body represents the horizontal part of the cleat (rigid body number 2 in the figure). A mass is attached to rigid body 2 in order to generate ground pressure. The independent nodes of the bodies are related to each other, such that no relative motion in displacement direction can occur. The interface properties between the bodies and the soil can be found in Table 3. This strategy showed very good convergence behavior. The contact surface to the soil is designed to include friction using the Mohr-Coulomb friction model as described in [19]. The analysis process is divided into a preanalysis and a main analysis. The preanalysis uses a modified model to determine the displacements of the nodes at the bottom side of the cut-out. In addition to the blade rigid body, another rigid body is inserted at the cut-out interfacing with the bottom side. It has the same mass of the soil, which is missing at the cut-out. Applying gravity load to the model will now result in a homogenous displacement field. The displacements of the bottom side nodes are then passed to the main analysis and represented by static displacements. The main analysis is an implicit finite element analysis. The rigid bodies are displaced in small steps towards the +X direction. During each displacement step, many equilibrium iterations are performed in order to account for the nonlinear material behavior. After each step, the total force is read-out and stored. The analysis stops, as soon as there is no significant increase in the reaction force.

Table 1: Parameters A and B depending on the type of surface surrounding the Mohr-Coulomb yield surface.

Type of Mohr-Coulomb conversion	Parameter A	Parameter B
Circumscribes	$\frac{6\cdot c\cdot\cos(\phi)}{\sqrt{3}\cdot(3-\sin(\phi))}$	$\frac{2\cdot\sin(\phi)}{\sqrt{3}\cdot(3-\sin(\phi))}$
Middle-circumscribes	$\frac{6\cdot c\cdot\cos(\phi)}{\sqrt{3}\cdot(3+\sin(\phi))}$	$\frac{2\cdot\sin(\phi)}{\sqrt{3}\cdot(3+\sin(\phi))}$
Incribes	$\frac{3\cdot c\cdot\cos(\phi)}{\sqrt{9+3\cdot\sin(\phi)^2)}}$	$\frac{\sin(\phi)}{\sqrt{9+3\cdot\sin(\phi)^2)}}$

[DP_Parameters].

2.2.3. Numerical Sizing Process of a Complete Spaced-Link Track. If the spaced link track is used for tracks, it is of major importance to choose the spacing between the cleats, such that the soil failure in front of each cleat does not affect the next cleat. If not, the spaced link track design would become a conventional one. Figure 2 in the previous chapter is

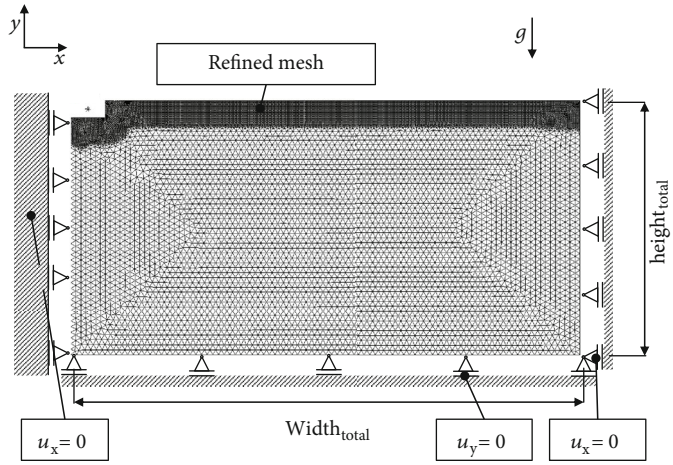

Figure 4: Overview of the FEM model with boundary conditions, dimensions, and global interface to rigid body.

Table 2: Soil properties and references used for the finite element model.

Soil parameter	Size	Unit	Reference
E-modulus	50 000	[MPa]	Derived from [20]
Poisson ratio	0.2	[-]	Derived from [20]
Density	1540	$[kg/m^3]$	[22]
Cohesion	1034	[Pa]	[22]
Friction angle	29.3	[deg]	[22]

illustrating a track with sufficient spacing (b) and one with zero spacing (a). The soil failure line on the conventional track (a) is described by the line connected by the points C-A-B, which is similar to a turned around cup design. The spacing between the cleats (l_s) depends on the cleat geometry s_s and the load on each cleat. Driven by l_s, the number of cleats can be calculated depending on the total length l_{total} and the cleat dimension s_s(see equation (9)). The number of cleats on a track with a given length and a total load is calculated iteratively as the final spacing and load per cleat is not known in advance. A new iterative sizing process is used to determine the track resistance of a single track. The sizing process uses the total length (l_{total}), the cleat and track dimensions and the load per track ($m_{track}g$) as input. The process can be described as follows:

(i) Assume l_s

(ii) Derive N_s using equation (9)

(iii) Derive mass per cleat using m_{track}/N_s

(iv) Build and solve FEM model

(v) Read-out l_s

(vi) Compare the assumed and calculated values for l_s, replace l_s by the new results and repeat steps 2. to 5. until l_s remains similar

(vii) Read-out force per cleat and derive total force

By using this approach the spacing of the track and the number of the cleats is automatically adjusted to the parameter of the global track.

2.2.4. Slippage Resistance Estimation of a Three-Dimensional Foot. The result of the numerical analysis is a specific force per unit-width (F_{spez}) and the adjacent l_s. The force generated by the reference foot is then calculated by:

$$F_{BST} = N_s\, b_s\, F_{spez}, \tag{8}$$

with

$$N_s = \frac{l_s + (a_{contact}/b_s)}{l_s}. \tag{9}$$

2.2.5. Material Properties. Sandy loam is used as material. This is mainly driven by drag measurements of the spaced-link track performed by Bekker in this soil. Bekker published cohesion and the friction angle of the soil together with the results of his measurements. The E-Modulus and poisson ratio needed for the numerical analysis were not published. Sandy loam consists of clay, sand, and silts in a variable fraction. The individual numbers of E-modulus and poisson ratio for the materials were shown in [20]. Based on the given composition of sandy loam derived from the soil texture triangular [21], a bandwidth of numbers for the unknown properties is derived: The E-modulus can vary between 4.4 and 114.8 MPa; The poisson ratio can vary between 0.16 and 0.5. Several analyses were performed with different numbers within this bandwidth, until the best fit to the measurements is achieved. The final numbers are shown in Table 2.

2.2.6. Review of the Analytical, Numerical, and Experimental Results. Bekker performed field testing of the spaced-link track using a small track vehicle called the "groundhog". This vehicle has two tracks, each with a width of 36 in. and a total length of 108 in. The cleats have a dimensions of 4 in.× 4 in. ($h_s \times s_s$). The spacing (l_s) is 14 in. He measured the total track

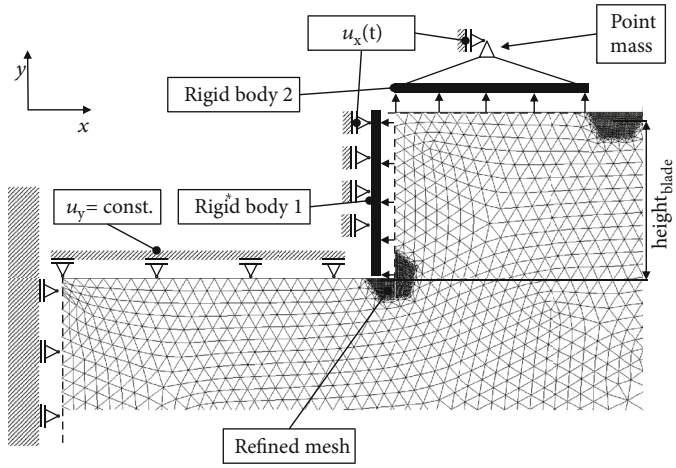

Figure 5: Detailed view of the modelling of a single cleat in soil.

Table 3: Contact properties used for finite element model.

Property	Size	Unit
Soil-metal friction coefficient	0.3	[-]
Penalty stiffness	1e10	[-]
Tangential stiffness	1e10	[-]

[contactproperties].

force H_{total} for different loads and compared the measurements to his analytical results. (Details about the test can be found in [5]).

With the given dimensions, the numerical model is used to derive the results of the total track force for the same loads as specified in [5]. Figure 6 shows the numerical results, the measured results, and the analytical results presented by Bekker. The average deviation of the numerical results from the measured values is approx. 3%. The deviation of Bekker's analytical results is slightly higher. The numerical model estimates the total track force especially for higher loads very well. The analytical results are correct for the middle range of loads, but overestimate the track for higher and lower ground pressures. With these results, the numerical model is verified to be used for further studies. The results furthermore underline the better accuracy of the numerical model at higher ground pressure.

3. Comparison between the HP^3 Design and Bekker's Spaced-Link Track Design

3.1. The Current Design (HP^3). The HP^3 instrument uses four, rigid feet as a contact interface to the soil. A bottom view of one single foot is shown in Figure 7. The design is deeply investigated by [4]. It is based on a circular turned-around cup shape, which sinks into the ground completely during operation. The force against the slip of this design can be approximated by the combination of the force from the shear failure area underneath the foot (a_{contact}) and the bulldozing force in front of the foot in track direction. The shear failure underneath the foot is analytically determined based on the Mohr-Coulomb failure criterion, which was applied to tracks by [23] before. It is given by:

$$F_{\text{Mohr-Coulomb}} = a_{\text{contact}}\, c + m_{\text{total}}\, g\, \tan\phi. \tag{10}$$

The total mass at the shear failure plane (m_{total}) is the combination of the foot load and the soil enclosed within the geometry of the foot (m_{soil}) (see equation (11)).

$$m_{\text{total}} = m_{\text{soil}} + m_{\text{foot}}. \tag{11}$$

The bulldozing force generated by one foot is determined specifically for a unit-width blade. The specific force is then integrated in track direction at the outer edge of the foot. The specific force can be estimated by equations presented by [23] (neglecting surcharge):

$$F_{\text{BD}} = \left(\gamma_s {h_b}^2 K_\gamma + c h_b K_{ca} - \gamma_s h_b^2 K_s e^{-S}\right), \tag{12}$$

with the soil scale index S:

$$S = \frac{c}{\gamma_s\, h_b}. \tag{13}$$

K_{ca}, K_γ, and K_s are empirical factors, which are published together with the equation by [23]. h_b describes the height of the blade, c the cohesion, and γ_s the unit weight of the soil. The force generated by the HP^3 foot design can be then estimated by integrated the specific force from bulldozing at the outer radius of the foot (R) and the force generated by shear failure underneath the foot:

$$F_{\text{HP3}} = \int_{\phi 1}^{\phi 2} F_{\text{BD}} \cos(\phi) R\, d\phi + a_{\text{contact}} c + (m_{\text{soil}} + m_{\text{foot}}) g \tan\phi. \tag{14}$$

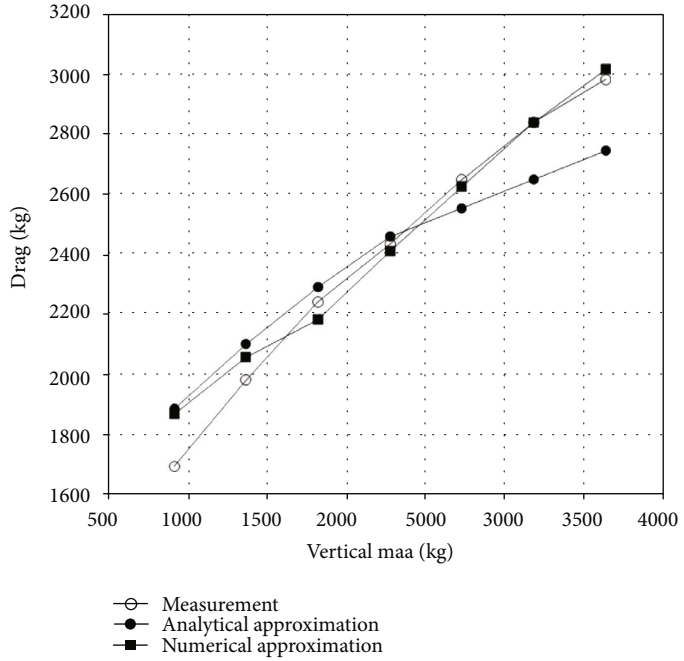

Figure 6: Comparison of the total drag between measurement, analytical results (both reprinted from [22]) and numerical results for the "ground-hog".

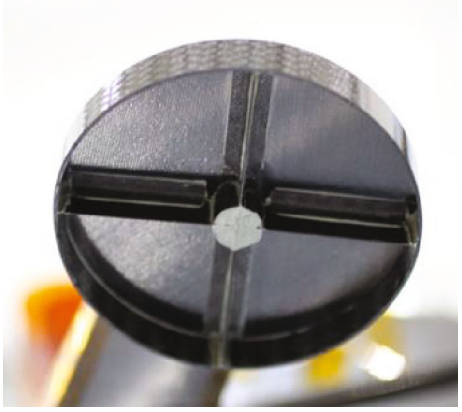

Figure 7: Bottom view of one HP^3 flight-model foot.

Table 4: Results of the numerical analysis of single cleats with unit-width of Bekkers spaced-link track for Earth and Mars gravity.

Contact area	Force (Earth) [N/mm]	l_s (Earth) [mm]	Force (Mars) [N/mm]	l_s (Mars) [mm]
250	0.117	41.5	0.0865	27.5
750	0.089	26.5	0.071	19.5
1500	0.079	21.5	0.066	17.25
2500	0.075	18.5	0.06	15.5

Integrated between $\phi_1 = -90$ deg and $\phi_2 = +90$ deg. This results in:

$$F_{\mathrm{HP3}} = 2F_{\mathrm{BD}}R + \pi R^2 c + (m_{\mathrm{soil}} + m_{\mathrm{foot}})g \tan\phi. \quad (15)$$

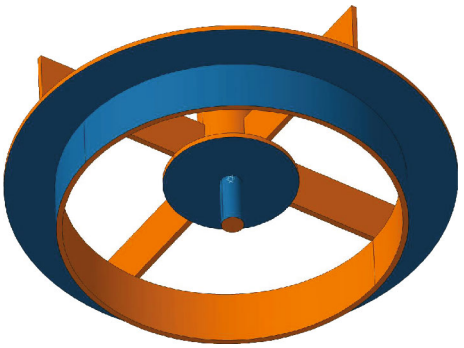

Figure 8: Bottom view of a foot equipped with two cleats.

3.2. The Modified Spaced-Link Design. The HP^{3}design shall be replaced by a design based on Bekker's spaced-link track to generate more force against slip. The given volume and outer shape shall remain the same, as those are the result of the available volume on the lander deck. The available space is circular with a diameter of about 80 mm at available depths of 10 mm. Hence, the linear cleat design of Bekker's track needs to be transformed into a circular design feasible with the given volume. First, the baseline design was transformed by modifying the brim of the current foot design such that it resembles a cleat. It was investigated secondly, how the remaining inner diameter can be used for further cleats: At a cleat ratio of 1 : 1 (depths to height), the available diameter becomes 60 mm. The required spacing between the cleats is between 16 and 19 mm at a contact area of 2200 mm^2 (see Table 4). Considering also the cleat geometry itself (another 10 mm), the needed space would consume nearly all available space. Figure 8 illustrates this problem. The remaining space at the

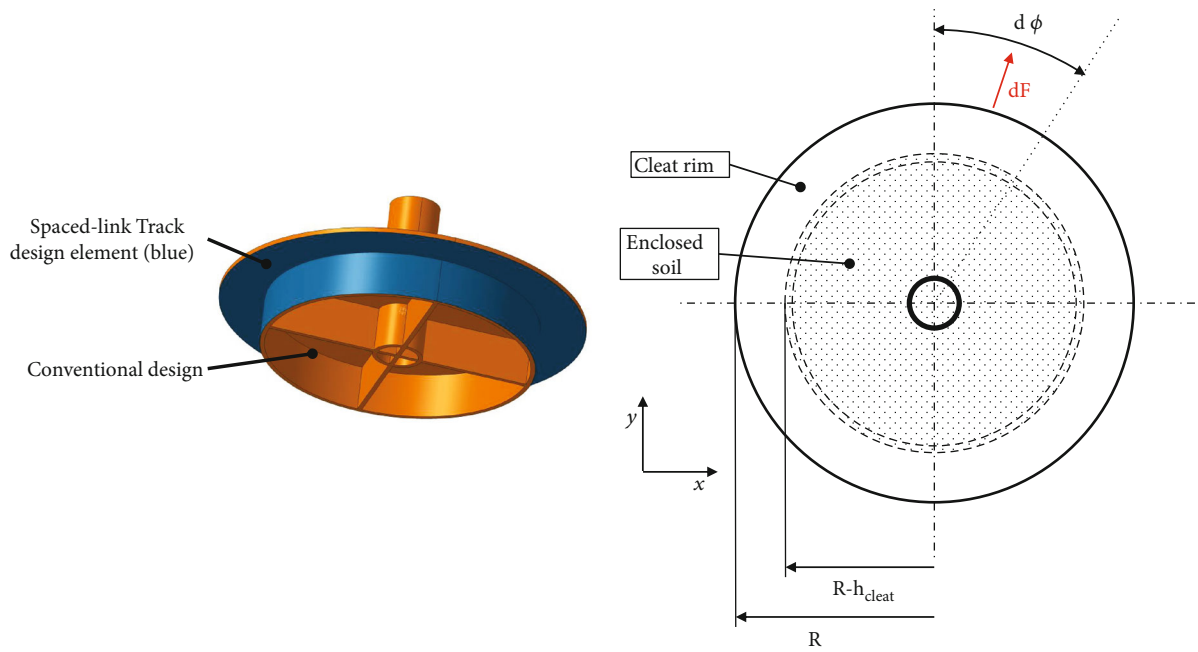

Figure 9: Schematic top view of the new proposed design.

center of the foot is just enough to be filled by a thin pin structure. This pin/cleat structure would only generate very little slippage resistance as its diameter is very small (see equation (16)). The inner part of the feet is therefore designed like a turned-around cup shape instead (see Figure 9).

Same as the original design, this foot design uses a cylindrical strut as an interface to the structure of the instrument located at the center of the foot. The length of the strut can be adjusted to the needed space between the bottom part of the instrument and the soil. The material thickness of the side walls is kept as thin as possible to ensure a sufficient sinkage of the instrument into the soil. The performance is estimated with a similar approach as for the current design: The specific forces per unit-width are estimated numerically with the model described in Section 2.2. The results are shown in Table 4. The results are based on a constant mass of 0.825 kg (mass per foot of HP^3) at a variable contact area. This specific force is integrated at the edge of the foot pointing into track direction. The force from the enclosed soil is analytically determined using the Mohr-Coulomb failure criterion in accordance to equation (10). A top view of the foot and the annotations can be found in Figure 9.

$$F_{\text{spaced-link}} = \int_{\phi_1}^{\phi_2} F_{\text{spez}} \cos(\phi)(R - h_{\text{cleat}})d\varphi + \pi(R - h_{\text{cleat}})^2 c + (m_{\text{soil}} + m_{\text{foot}})g \tan\phi. \quad (16)$$

Integrated between $\phi_1 = -90$ deg and $\phi_2 = +90$ deg. This results in:

$$F_{\text{spaced-link}} = 2F_{\text{spez}}(R - h_{\text{cleat}}) + \pi(R - h_{\text{cleat}})^2 c + (m_{\text{soil}} + m_{\text{foot}})g \tan\phi. \quad (17)$$

4. Results

Figure 10 illustrates the generated track force of both designs at different gravities (Mars and Earth) and potential foot diameters. The dotted lines represent the results for Mars gravity; the full lines represent the results for Earth gravity. The parameters for the analysis have been selected from Table 2. The 80 mm foot diameter has been extrapolated based on the given results.

The generated force increases with the available foot diameter. This result can be explained by the larger circumference of the foot, which increases the area used for bulldozing (HP^3) and for the spaced-link designed edge. This effect is further explained by the significant larger available area for cohesion. The generated force under Earth gravity is higher than the force under Mars gravity. Gravity contributes linearly to the Mohr-Coulomb terms of the used equations, and it also contributes linearly to the force generated by bulldozing in front of the foot. Hence, a change in gravity also has a significant influence on the total generated force. The graphs clearly indicate that the currently used design has better efficiency than the new proposed design in terms of slippage resistance. The generated force by the currently used design is up to 50% larger than the force generated by a foot based on the spaced-link track. This effect is present for both studied gravities. The specific bulldozing force can be estimated by equation (12). Using the soil parameters from Table 2 and the empirical factors from [23], one can calculate the specific bulldozing force to 87.7 N/m for Earth and 86.7 N/m for Mars gravity. The specific force remains constant regardless on the

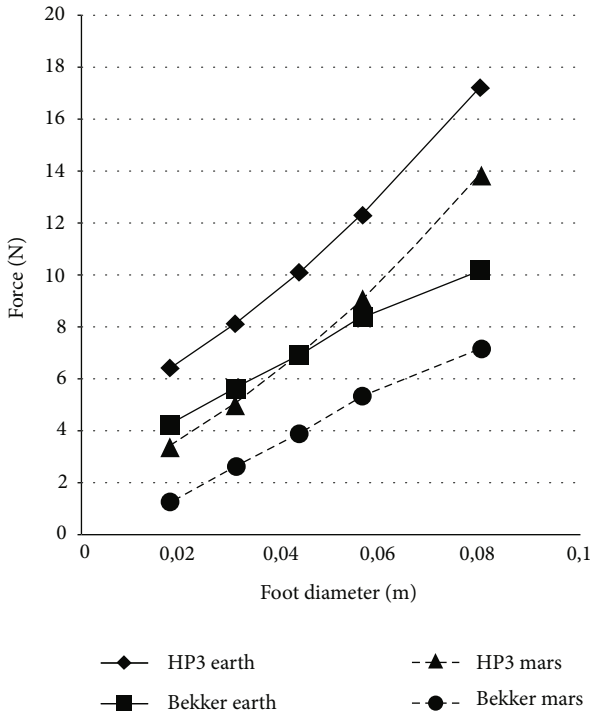

Figure 10: Results of the design study.

selected foot diameter. The specific force generated by the front of the foot of the spaced-link track design is high at very small areas, but drops significantly towards larger contact areas. The spaced-link track design only generates more force at very small areas under Earth gravity. The enclosed soil area of the spaced-link track design is significantly smaller, which reduces additionally the generated force. Both effects together decrease the efficiency of the proposed design significantly.

5. Conclusion

The paper studied a new design idea to increase the slippage resistance of successors of the Mars instrument HP^3. The design idea is based on Bekker's spaced-link track. The analytical equations to determine the force generated by a track are recapitulated. The analytical equations are based on many empirical parameters, and the accuracy is not known for other gravities and small scales. Therefore, a numerical model based on the FEM is introduced and verified based on experimental results published by Bekker. A new foot design based on the spaced-link track is proposed. The analytical estimation to determine their slippage resistance is presented and used to determine their efficiency for different foot diameters. It turned out that the efficiency of the new design is very low, and it can therefore not compete with current used design. This discards the design from further studies of foot designs for this instrument. But it shall be pointed out here that this is mainly driven by the available little space. Applying the design idea to future instruments with more space available is reasonable as more cleats can be used. This might make the design competitive with other.

Data Availability

The data can be requested by contacting the corresponding author.

Disclosure

The manuscript has not been published and is not under consideration for publication in any other journal.

Conflicts of Interest

We have no conflicts of interest to disclose.

References

[1] T. Spohn, M. Grott, S. E. Smrekar et al., "The heat flow and physical properties package (Hp^3) for the Insight mission," *Space Science Reviews*, vol. 214, no. 5, article 96, 2018.

[2] W. B. Banerdt and C. T. Russell, "Editorial on: topical collection on Insight mission to Mars," *Space Science Reviews*, vol. 211, no. 1-4, pp. 1–3, 2017.

[3] A. Trebi-Ollennu, W. Kim, K. Ali et al., "InSight Mars lander robotics instrument deployment system," *Space Science Reviews*, vol. 214, no. 5, article 93, 2018.

[4] S. Reershemius and T. L. Hudson, "Design and Verification of the Feet Design used for the "Heat Flow Property Package Instrument" (HP^3) on-board the Mars Mission InSight," *Advances in Space Research*, vol. 65, no. 10, pp. 2290–2302, 2020.

[5] M. G. Bekker, *Off-the-Road Locomotion: Research and Development in Terramechanics*, University of Michigan Press, 1960, https://books.google.de/books?id=uHdTAAAAMAAJ.

[6] NASA, *Images*, NASA, 2018, https://mars.nasa.gov/insight/multimedia/images/.

[7] K. Terzaghi, *Theoretical Soil Mechanics*, Wiley, 1943.

[8] A. Armin, R. Fotouhi, and W. Szyszkowski, "On the FE modeling of soil-blade interaction in tillage operations," *Finite Elements in Analysis and Design*, vol. 92, pp. 1–11, 2014.

[9] M. Abo-Elnor, R. Hamilton, and J. T. Boyle, "3D Dynamic analysis of soil-tool interaction using the finite element method," *Journal of Terramechanics*, vol. 40, no. 1, pp. 51–62, 2003.

[10] J. M. Fielke, "Finite element modelling of the interaction of the cutting edge of tillage implements with soil," *Journal of Agricultural Engineering Research*, vol. 74, no. 1, pp. 91–101, 1999.

[11] Krabbenhoft, *Basics Computational Plasticity*, Department of Civil Engineering, Technical University of Denmark, 2002.

[12] J. F. Labuz and A. Zang, "Mohr-Coulomb failure criterion," *Rock Mechanics and Rock Engineering*, vol. 45, no. 6, pp. 975–979, 2012.

[13] S. A. B. da Fontoura, "Lade and modified lade 3D rock strength criteria," *Rock Mechanics and Rock Engineering*, vol. 45, no. 6, pp. 1001–1006, 2012.

[14] H. Matsuoka and T. Nakai, "Stress-deformation and strength characteristics of soil under three different principal stresses," *Proceedings of the Japan Society of Civil Engineers*, vol. 1974, no. 232, pp. 59–70, 1974.

[15] D. V. Griffiths and J. Huang, "Observations on the extended Matsuoka–Nakai failure criterion," *International Journal for*

Numerical and Analytical Methods in Geomechanics, vol. 33, no. 17, pp. 1889–1905, 2009.

[16] L. R. Alejano and A. Bobet, "Drucker–Prager criterion," *Rock Mechanics and Rock Engineering*, vol. 45, no. 6, pp. 995–999, 2012.

[17] D. C. Drucker and W. Prager, "Soil mechanics and plastic analysis or limit design," *Quarterly of Applied Mathematics*, vol. 10, no. 2, pp. 157–165, 1952.

[18] H. Jiang and Y. Xie, "A note on the Mohr-Coulomb and Drucker-Prager strength criteria," *Mechanics Research Communications*, vol. 38, no. 4, pp. 309–314, 2011.

[19] ANSYS, *ANSYS Academic Research Mechanical, Release 16.1*, ANSYS Help System, 2007.

[20] J. E. Bowles, *Foundation Analysis and Design*, McGraw-Hill, 1996.

[21] Ditzler, Monger, and Scheffe, *Soil Survey Manual (Ssm)*, United States Department of Agriculture, 2017.

[22] R. D. Nelson and E. T. Selig, "Bulldozing resistance of plane blades in cohesionless soil," in *SAE Technical Paper Series*, USA, 1964.

[23] J. Y. Wong, *Terramechanics and Off-Road Vehicle Engineering: Terrain Behaviour, Off-Road Vehicle Performance and Design*, Elsevier Science, 2009.